When does sampling uncertainty matter in matrix population models? Evidence from published projection matrices

Authors

Owen R. Jones*[1,2], Emily G. Simmonds[2]

Affiliations

[1] Department of Biology, University of Southern Denmark, Odense, Denmark

[2] Institute of Ecology and Evolution, School of Biological Sciences, University of Edinburgh, Edinburgh, UK

Corresponding author

* Owen R. Jones, jones@biology.sdu.dk

Abstract

1. The collation of thousands of population projection matrices in the COM(P)ADRE Matrix Databases has enabled large-scale comparative analyses in ecology, evolution, and demography. A persistent challenge is that transition rates are estimated from finite samples, yet the resulting sampling uncertainty is rarely reported and typically ignored in downstream analyses. Although sampling uncertainty is well recognised, it remains unclear when it affects demographic inference.

2. Using a subset of studies from the COMPADRE Plant Matrix Database for which transition-specific sample sizes could be obtained, we reconstructed sampling distributions for transition rates and derived demographic parameters, and conducted three related analyses: a comparative analysis, a within-species time-series analysis, and a multi-site extension of the climate-demography analysis, each fit with and without explicit sampling uncertainty.

3. The effects of sampling uncertainty were strongly trait-dependent. It had little influence on integrated demographic metrics such as population growth rate, but accounted for a substantial fraction of the total variation in traits related to mortality trajectories, particularly the shape of the mortality distribution. In these cases, point estimates were often systematically displaced from their underlying sampling distributions due to boundary estimates of stage-specific survival (i.e. survival probabilities near 0 or 1), which are common in published matrices. By contrast, inference in a within-species analysis of weather effects on vital rates was largely unaffected.

4. Together, these analyses show that ignoring sampling uncertainty does not universally compromise inference from published projection matrices, but can yield fragile or biased conclusions for certain demographic traits. We identify structural features of MPMs and

analyses that may indicate heightened sensitivity to sampling uncertainty, and discuss implications for researchers using compiled demographic databases.

Keywords: age-from-stage methods; parametric bootstrapping; estimation bias; parameter uncertainty; stage-structured models; sensitivity analysis; plant demography; life history traits

Introduction

The collation of published demographic data in databases such as PanTHERIA (Jones et al. 2009), AnAge (de Magalhães and Costa 2009), Myhrvold et al.'s (2015) amniote life-history database, and COM(P)ADRE (Salguero-Gómez et al. 2015, Salguero-Gómez et al. 2016a) has enabled fascinating comparative analyses in ecology, evolution, and demography (e.g. Garratt et al. 2013, Adler et al. 2014, Healy et al. 2014, Fristoe et al. 2017). By leveraging open-source databases that aggregate data from hundreds of individual studies, researchers can test hypotheses of interest across taxonomic, spatial, and temporal scales that would otherwise be impossible. However, analyses based on published demographic results rather than underlying raw data also present their own challenges.

One challenge in working with large collections of published data is understanding and modelling the sources of underlying uncertainty. For instance, the demographic parameters reported in the databases noted above have almost always been estimated from a sample of individuals drawn from a larger population of interest, and therefore carry inherent sampling uncertainty. However, parameter-specific sample sizes and standard errors are rarely available and are often difficult to obtain even from the original data sources. These original studies, which produce the parameter estimates later compiled in demographic databases, usually account for sampling uncertainty in their own analyses, but uncertainty is often not reported in a form that can be propagated from the published matrices. Therefore, studies that subsequently analyse parameter estimates compiled in demographic databases rarely incorporate this uncertainty, raising questions about the robustness of resulting inferences (Caswell 2001, Ch. 12; Biggs et al. 2009).

Despite widespread recognition that sampling uncertainty is inherent in demographic estimates (Caswell 2001), a key unresolved question concerns when this uncertainty materially affects inference from compiled databases. Comparative analyses using projection matrices rely on a

diverse set of derived demographic traits, ranging from highly integrated metrics such as population growth rate to traits that depend on long-term survivorship or tail behaviour, such as life expectancy or the shape of mortality trajectories. Whether these different classes of traits are equally sensitive to sampling uncertainty under typical data regimes remains poorly understood.

Recent work has reviewed the importance of uncertainty propagation in matrix population models and outlined best-practice guidelines for addressing it (Simmonds and Jones 2024). That paper focused on methodology and characterised the sources of uncertainty, the available propagation techniques, and recommendations for practice, but did not empirically quantify the consequences of ignoring uncertainty across a range of real analyses and demographic traits. Here, we address that complementary question directly: not how uncertainty should be handled, but when handling it actually changes the conclusions researchers draw from published projection matrices.

We investigate sampling uncertainty in the COMPADRE Plant Matrix Database (Salguero-Gómez et al. 2015; www.compadre-db.org), which currently contains over 9,000 matrix population models (i.e. projection matrices, hereafter MPMs) drawn from more than 650 studies. Over the course of its development, researchers have used COMPADRE (and the sister animal matrix database COMADRE; Salguero-Gómez et al. 2016a) to address diverse topics in ecology, evolution, and demography, including studies of the structuring of life-history variation (Franco and Silvertown 1996, Salguero-Gómez et al. 2016b), comparative analyses of ageing (Baudisch et al. 2013, Jones et al. 2014), tests of the demographic buffering hypothesis (McDonald et al. 2017), and analyses of the impact of climate on population dynamics (Coutts et al. 2016, Csergő et al. 2017). In practice, these analyses involve deriving parameters from a set of MPMs in COMPADRE (e.g. equilibrium population growth rate λ, elasticities of λ, reproductive values, mean vital rates, generation time, life expectancy), and incorporating these parameter estimates, or further derivations, into a statistical model.

Our aim is to examine how sampling uncertainty in published projection matrices propagates to specific MPM-derived quantities and to explore when point estimates are robust or fragile. We expect sensitivity to vary systematically across traits, reflecting a spectrum from highly integrated metrics — such as population growth rate, which averages over many transitions and should be buffered against uncertainty in any single element — to traits that depend on long-term survivorship inferred indirectly via age-from-stage methods, such as life expectancy and mortality shape, where small errors in late-stage survival can amplify into large errors in derived quantities. We structure our three analyses to bracket this spectrum deliberately. The focal quantities are mature life expectancy, the shape of the mortality trajectory, log population growth rate, and recruitment-climate regression coefficients. Because COMPADRE does not routinely include transition-level sample sizes, our analysis is restricted to the subset for which these data could be assembled (695 MPMs from 31 studies; details in Methods). We illustrate trait-dependent uncertainty effects using a multi-species comparative analysis of life expectancy-shape relationships (analysis 1), a single-species time-series analysis of weather effects on recruitment (analysis 2), and a multi-site extension of the same climate-demography framework (analysis 3), and use these to identify diagnostic features that help researchers assess robustness in their own work.

Methods

Background on the COMPADRE Plant Matrix Database

The COMPADRE database includes MPMs and associated metadata from published studies dating back to 1966 (Salguero-Gómez et al. 2015). Where possible, MPMs are decomposed into component processes of survival, growth, and retrogression (the U matrix), sexual reproduction (F), and clonal reproduction (C). The database provides a range of metadata for each MPM, including the relevant time period, geographic coordinates of the study site, population or site

identifiers, and treatment conditions. From a given source study, COMPADRE often contains multiple MPMs reflecting different sites, time periods, and/or treatment conditions, as well as one or more "mean MPM" calculated as an element-by-element arithmetic mean across multiple years and/or sites.

Target studies

We used an earlier version of COMPADRE to identify an initial group of 86 studies from which we sought data, applying the following criteria: studies published from 2010 onwards; species of common perennial growth forms (herbaceous, shrub, tree, palm, and succulent); wild populations not subjected to experimental treatments; and MPMs with three or more stage classes and a one-year projection interval. Data collection and analysis were subsequently conducted using COMPADRE version 6.26.3.0 (created Mar_11_2026). Of the 86 initially identified studies, we obtained the data required to model sampling uncertainty for 26: most exclusions reflected insufficient reporting of transition-specific sample sizes, and a small number used estimation methods incompatible with our bootstrapping approach (e.g. mark-recapture or multi-stage vital rate products). We cannot rule out selection bias, but have no strong reason to expect systematic differences between included and excluded studies. The 26 studies yielded 580 MPMs for 116 populations of 25 species. We supplemented this set with 5 additional studies published before 2010 for which we had previously obtained data (targeted based on a criterion of at least 4 years of temporal replication), giving a final set of 31 studies representing 695 MPMs for 132 populations of 30 species.

Typical construction of matrix population models

A matrix population model A is a square projection matrix whose elements A_{ij} represent estimated transition rates from stage class j to stage class i over one projection interval (typically one year). Transitions may reflect the passage of individuals from one stage to another through

survival, growth, or retrogression (the U component), or the production of new individuals via reproduction (the F component); $A = U + F$. Sometimes the reproductive transitions are further split into sexual and clonal contributions.

The methodology for estimating transition rates varies across studies. In plant MPM studies, survival-related transitions are often estimated from observed stage transitions of marked individuals between censuses, as in Eq. (1); in other systems, especially mobile animals, transition and survival estimation more commonly uses models that explicitly account for imperfect detection.

$$U_{ij,t} = \frac{\text{number transitioned from stage } j \text{ in year } t-1 \text{ to stage } i \text{ in year } t}{\text{number in stage } j \text{ in year } t-1}. \qquad (1)$$

Reproductive transitions are sometimes estimated directly from counts of new recruits at time t per reproductive individual at time $t-1$, as in Eq. (2),

$$F_{sr,t} = \frac{\text{number in recruit stage } s \text{ in year } t}{\text{number in reproductive stage } r \text{ in year } t-1}. \qquad (2)$$

The demographic interpretation of F depends on census timing and stage definitions (e.g. pre-breeding vs post-breeding formulations). Here, Eq. (2) is a count-based estimator of the recruit transition across one projection interval and we use the published matrix entries as represented in COMPADRE rather than reparameterising each study to a single census convention.

Alternatively, reproductive transitions may be split into multiple lower-level vital rates (e.g. numbers of flowers per plant, fruits per flower, and seeds per fruit, seed survival probability, and seed germination probability), which are typically estimated from separate samples, and then multiplied to derive the overall transition rate. In some studies, transition rates are estimated using more nuanced statistical models that partially pool estimates across stage classes, sites, and/or years, or incorporate additional variables external to the MPM.

Sampling distribution for a single MPM

Techniques for estimating sampling uncertainty in transition rates and derived parameters are reviewed in Caswell (2001, Ch. 12). The method we use here is parametric bootstrapping, in which we generate a sampling distribution for each MPM by taking 2,000 independent random draws from the sampling distribution of each underlying transition rate. For example, if U_{ij} is a survival-related transition from stage j to i, estimated from the observation that k out of the n individuals in stage j survived and transitioned to stage i (and the remaining $n - k$ died), we can model the U_{ij} transition as a binomial sample with k successes in n trials. We could equivalently use a multinomial likelihood here (given observed counts x_m of each possible outcome m), which flexibly scales to instances with more than two possible outcomes (e.g. an individual from stage j might die, survive and remain in stage j, or survive and grow to stage $j + 1$). For reproductive transitions, we use a Poisson likelihood to model the number of recruits k produced by a given number of reproductive individuals n. We distinguish structural zeros (biologically impossible transitions) from sampling zeros (possible but unobserved transitions): structural zeros are fixed at 0 in all bootstrap draws, whereas sampling zeros are modelled with the same likelihood-based uncertainty framework as non-zero transitions.

Analyses

We chose parametric bootstrapping because the sampling distributions of survival and reproductive transitions follow well-characterised probability models (multinomial and Poisson, respectively) whose parameters can be directly estimated from the transition frequencies reported in source studies. This makes parametric bootstrapping more tractable than MCMC for our scale of analysis and more principled than the empirical bootstrap, which cannot generate variation when all individuals in a stage class experience the same outcome (e.g. all survive), a situation common in published matrices. When a stage-specific sample size was recovered as

zero, we retained the published point-estimate transition column unchanged in all bootstrap draws rather than treating it as a structural zero. In such cases, the matrix remains usable in the same way it would be in a comparative database analysis, but no additional sampling variation is propagated for that unsupported column.

Illustrative example

We illustrate with an MPM for the perennial forb *Agrimonia eupatoria* (Rosaceae) from a study carried out in southern Sweden (Kiviniemi 2002) (Population 'B'; projection interval 1997-1998). The full matrix is

$$A = \begin{bmatrix} 0 & 0 & 0 & 0.19 \\ 0.86 & 0.78 & 0 & 0 \\ 0.06 & 0.67 & 0.28 & 0 \\ 0 & 0 & 0.22 & 0.70 \end{bmatrix}.$$

Decomposed into survival/growth (U) and reproduction (F) components:

$$U = \begin{bmatrix} 0 & 0 & 0 & 0 \\ 0.86 & 0.78 & 0 & 0 \\ 0.06 & 0.67 & 0.28 & 0 \\ 0 & 0 & 0.22 & 0.70 \end{bmatrix}, \quad F = \begin{bmatrix} 0 & 0 & 0 & 0.19 \\ 0 & 0 & 0 & 0 \\ 0 & 0 & 0 & 0 \\ 0 & 0 & 0 & 0 \end{bmatrix}.$$

In that study, ~80 plants were monitored each year in a population estimated at ~1000 individuals. Mirroring the $A = U + F$ decomposition above, the observed transition frequencies can be written as:

$$N_U = \begin{bmatrix} 0 & 0 & 0 & 0 \\ 12/14 & 14/18 & 0 & 0 \\ 0 & 1/18 & 6/9 & 13/47 \\ 0 & 0 & 2/9 & 33/47 \\ 2/14 & 3/18 & 1/9 & 1/47 \end{bmatrix},$$

$$N_F = \begin{bmatrix} 0 & 0 & 0 & 9/47 \\ 0 & 0 & 0 & 0 \\ 0 & 0 & 0 & 0 \\ 0 & 0 & 0 & 0 \end{bmatrix}.$$

Here, columns index origin stage j; rows 1-4 in N_U index destination stages, and the extra row d contains stage-specific death frequencies. The N_F matrix remains 4×4 and contains only reproductive transitions. From these counts, the sampling distributions of the underlying transition rates are:

$$(12,2) \sim \text{Multinomial}(U_{21}, U_{d1}),$$

$$(14,1,3) \sim \text{Multinomial}(U_{22}, U_{32}, U_{d2}),$$

$$(6,2,1) \sim \text{Multinomial}(U_{33}, U_{43}, U_{d3}),$$

$$(13,33,1) \sim \text{Multinomial}(U_{34}, U_{44}, U_{d4}),$$

$$9 \sim \text{Poisson}\big(\exp(F_{14} + \log 47)\big).$$

To create a sampling distribution for the focal MPM, we take 2,000 independent draws from the sampling distributions implied above (see Supplementary Methods section S1.1 for a full workflow description). At each iteration, we arrange the drawn transition rates into the form of our MPM and then use that MPM draw to calculate our derived parameter(s) of interest. After 2,000 iterations, we therefore have 2,000 independent draws from the sampling distribution of each transition rate and derived parameter.

The modest sample sizes underpinning this MPM (9-47 plants per stage class) result in relatively high sampling uncertainty in the transition rates (Fig. 1). For instance, the sample estimate for the vegetative-reproductive growth transition is 0.22 (2/9), but the upper bound of the 95% bootstrap interval suggests this transition rate could plausibly be as high as 0.45 in the population at large. Correspondingly, there is substantial sampling uncertainty in some derived parameters (Fig. 2). Based on the 95% bootstrap interval bounds, the equilibrium population growth rate could be as low as –17% per year or as high as +1% per year; life expectancy could be as low as

225 3.5 years or as high as 18.2 years; and the reproductive value of the vegetative stage class could
226 be 22% lower than that of the seedling stage or 1460% higher.

227 We chose three analyses to illuminate contrasting contexts in which sampling uncertainty may be
228 relevant. Analysis 1 is a comparative analysis across many species and populations, in which
229 derived traits depend heavily on long-term survivorship inferred indirectly from stage-structured
230 matrices, precisely the setting in which sampling uncertainty might compound. Analysis 2, by
231 contrast, is a within-species time-series analysis in which the response variable is a directly
232 observed count, the statistical model is closely tied to the raw data, and the question concerns an
233 environmental driver rather than a demographic trait per se. Analysis 3 extends analysis 2 to
234 multiple populations of the same species to assess whether inference robustness is consistent
235 across sites. Together, the three analyses bracket a range of typical uses of published MPMs and
236 allow us to ask whether the consequences of sampling uncertainty are consistent across contexts
237 or depend on the nature of the analysis.

238 *Analysis 1: Comparative analysis of mortality trajectories*

239 The analysis we focus on here tests the relationship between mature life expectancy and the
240 "shape" of the mortality distribution (sensu Baudisch 2011), where shape denotes the extent to
241 which mortality rates increase with age after reproductive maturity. Evolutionary biologists have
242 long been interested in variation in mortality trajectories within evolutionary theories of
243 senescence, but previous metrics used to compare rates of senescence may have conflated
244 variation in the shape of mortality trajectories with variation in the average level of mortality
245 (i.e. the inverse of life expectancy). Measures of shape proposed by Baudisch and colleagues
246 (Baudisch 2011, Baudisch et al. 2013, Wrycza et al. 2015) are mathematically independent of life
247 expectancy and therefore well-suited for comparative analyses. Whether shape is biologically
248 independent of life expectancy is a separate question, and an analysis by Baudisch et al. (2013)
249 (based on MPMs for 290 angiosperm species) found a positive relationship between life

expectancy and the shape of mortality trajectories. In addition to that analysis, several other studies have used estimates of life expectancy and shape derived from MPMs in COM(P)ADRE, primarily in studies of life-history variation (e.g. Salguero-Gómez et al. 2016b; Healy et al. 2019).

To estimate mature life expectancy (L) and shape (S), we first used age-from-stage methods (Cochran and Ellner 1992, Caswell 2001 Sec. 5.3) to derive a survivorship trajectory from each MPM, starting from the first stage class(es) with positive reproduction (see Supplementary Methods section S1.2 for details). We then estimated mature life expectancy by summing over the survivorship trajectory, as in Eq. (3),

$$L = \sum_{x} l_x \,, \qquad (3)$$

where l_x is the proportion of a cohort surviving from reproductive maturity to age x. To estimate shape, we used a metric proposed by Baudisch and Stott (2019), which compares the area under a survivorship trajectory to that under a reference trajectory assuming constant mortality with age. The metric can take any continuous value between –0.5 (maximal negative senescence; all individuals die at the age of maturity) and +0.5 (maximal senescence; all individuals die at the age of maximum longevity), with a value of 0 indicating a constant mortality rate (negligible senescence). Values of shape greater than, equal to, or less than zero correspond to Type I, II, and III survivorship curves, respectively. When deriving a survivorship trajectory from an MPM, the apparent mortality rate is guaranteed to approach a plateau as the stage distribution approaches its equilibrium (Horvitz and Tuljapurkar 2008). To avoid bias from artefactual mortality plateaus, we calculated shape from truncated survivorship trajectories, limited to the period before a cohort reaches its quasi-stable distribution (based on a distance threshold of 1%; see Supplementary Methods section S1.2).

We calculated life expectancy and shape at the population level, using one population-level MPM per population. For populations with temporal replication, we used a pooled population MPM if

available; otherwise, we used a population mean MPM; if neither was available, we constructed a population-level matrix by taking the element-wise mean of the available annual individual MPMs. When database records included both site-specific populations and aggregate population labels (e.g. combined multi-site entries), we retained the site-specific populations and excluded the aggregate rows to avoid double counting. To model sampling uncertainty for pooled or mean population-level MPMs, we pooled stage-specific sample sizes across years (see Supplementary Methods section S1.3). This approach ignores uncertainty arising from temporal variation in transition rates and therefore underestimates overall uncertainty in the pooled estimates. The degree of underestimation depends on how much transition rates vary across years relative to within-year sampling error; for species with high interannual variability, the bias could be substantial. Results should therefore be interpreted conservatively with respect to the influence of sampling uncertainty.

To model the relationship between point estimates of mature life expectancy and shape, we used a linear model with random intercepts at the species level (to account for non-independence among populations of the same species), as in Eq. (4),

$$y_{ij} \sim \text{Normal}\left(\alpha_j + \beta x_{ij}, \sigma^2\right), \qquad (4)$$

where x_{ij} and y_{ij} represent point estimates of life expectancy and shape, respectively, for population i and species j, α_j represent species-specific intercepts, β is the slope of the relationship between S and L, and σ^2 is residual variance. Species-level intercept variation is modelled as $\alpha_j \sim \text{Normal}(\mu_\alpha, \tau^2)$, where τ^2 is the among-species intercept variance (i.e., variance of random intercepts; distinct from residual variance σ^2). To incorporate sampling uncertainty, we used a measurement error model (based on McElreath 2020, sec. 14.1.2) where latent x_{ij} and y_{ij} are linked to sampling-distribution means ($\bar{x}_{ij}$ and $\bar{y}_{ij}$) and variances ($\sigma^2_{x,ij}$ and $\sigma^2_{y,ij}$) derived as described in the sampling-distribution section above, as in Eqs. (5), (6), and (7).

The structural form of the model is unchanged when sampling uncertainty is incorporated; Eqs. (5)-(7) restate the outcome model and add explicit sub-models for the true latent values of x_{ij} and y_{ij}, which are now treated as unknown quantities estimated from their bootstrap-derived sampling distributions rather than as fixed plug-in values:

$$y_{ij} \sim \text{Normal}\left(\alpha_j + \beta x_{ij}, \sigma^2\right), \qquad (5)$$

$$\bar{x}_{ij} \sim \text{Normal}\left(x_{ij}, \sigma^2_{x,ij}\right), \qquad (6)$$

$$\bar{y}_{ij} \sim \text{Normal}\left(y_{ij}, \sigma^2_{y,ij}\right). \qquad (7)$$

For these models, we used priors and settings as described in Supplementary Methods section S1.4.

In supplementary analyses, we estimated the variance components of life expectancy, shape, and other life history traits using a sampling-to-other variance ratio: the proportion of total observed variation in a demographic parameter attributable to transition-rate sampling uncertainty relative to variation from all other sources (principally biological variation among populations and species). For each parameter we partitioned total variance into a sampling component, estimated as the mean of the within-MPM sampling variances derived from the bootstrap distributions, and a residual component representing the remainder. A ratio greater than 1 indicates that sampling uncertainty exceeds biological variation; a ratio less than 1 indicates that biological variation dominates. Full details are given in Supplementary Methods section S1.5 and Supplementary Table S3.

Analysis 2: The impact of weather on demographic traits

We focus on a 12-year MPM time-series for *Silene spaldingii* (Lesica and Crone 2007), a perennial herb found in semi-arid grasslands of western North America. We selected this case because it provides a rare combination of multi-year temporal replication, recoverable transition-level

sample sizes, and matched local climate covariates, making it well suited for testing uncertainty propagation in a climate-response context. In that study, transition rates were estimated using the methods described above, as ratios of two integers (Eqs. (1) and (2)), and the corresponding stage-specific sample sizes are reported in Ellis et al. (2012). Eight of the MPMs in the 12-year time-series were non-ergodic due to missing estimates for the "rosette" stage class (i.e. no rosettes were observed in the sample plots). Instead of examining variation in population growth rates (which assumes ergodicity), we focus only on the reproductive transition (hereafter 'recruitment', the number of seedlings in year t per reproductive plant in year $t-1$). We note that recruitment estimated in this way is a relatively aggregated transition whose behaviour under sampling uncertainty may differ substantially from that of survival transitions, which are estimated from smaller stage-specific samples and are more prone to boundary estimates. The robustness we observe in this analysis therefore reflects properties of aggregate reproductive transitions under moderate sample sizes, and should not be taken as evidence that within-species analyses are always insensitive to sampling uncertainty.

We examined the effect of monthly temperature deviations, derived from PRISM monthly temperature rasters extracted at the study population coordinates (Daly et al. 2008; PRISM Group, Oregon State University 2026; Supplementary Methods section S1.6), on annual recruitment using a similar approach to Teller et al. (2016), in which we model separate slope coefficients for a series of K monthly lags (i.e., going back in time from the end of a given transition interval) in a way that allows smoothing of coefficients across nearby lags. The smoothing model we use here is a Gaussian process with an exponential covariance function, as in Eq. (8),

$$\log(y_t) \sim \text{Normal}\left(\alpha + \sum_k b_k\, x_{tk}, \sigma^2\right) \qquad (8)$$

with the monthly-coefficient prior and covariance structure given in Eqs. (9) and (10),

$$b \sim \text{MVN}(\mu_b, \mathbf{K}) \qquad (9)$$

and

$$K_{i,j} = \eta^2 \exp(-0.5\,\rho^2 (j-i)^2) \qquad (10)$$

respectively.

where y_t is annual recruitment in year t, and x_{tk} is the temperature deviation for year t at monthly lag k. Model parameters include the intercept (α), residual variance (σ^2), vector of monthly temperature coefficients (b), mean of the distribution of b (μ_b), covariance matrix ($\mathbf{K}$), maximum covariance for the b distribution (η^2), and the rate of decay in covariance with time (ρ^2).

In the model above, y_t represents a point estimate of annual recruitment derived from the relevant MPM. Recall that these values were initially calculated as the number of seedlings in year t divided by the number of reproductive adults in year $t-1$. To propagate sampling uncertainty, we model the raw seedling counts directly with a Poisson likelihood (Eq. (11)) and include $\log(N_{t-1})$ as an offset via the year-specific intercept model in Eq. (12), so expected counts scale with the number of reproductive plants sampled. Note that the two formulations also differ in model structure: the point-estimate model uses a Gaussian likelihood on log per-capita recruitment, whereas the uncertainty-aware model uses a Poisson likelihood on raw counts with a log-offset. Observed differences between formulations therefore reflect both structural change and uncertainty propagation, though in practice the two are virtually identical.

$$Y_t \sim \text{Poisson}\left(\exp\left(\alpha_t + \sum_k b_k\, x_{tk}\right)\right) \qquad (11)$$

year-specific intercepts

$$\alpha_t \sim \text{Normal}(\mu_\alpha + \log(N_{t-1}), \sigma_\alpha^2) \qquad (12)$$

This implies that uncertainty in per-capita recruitment declines with sample size: if $\hat{r}_t = Y_t/N_{t-1}$, then $\text{Var}(\hat{r}_t)$ scales as $1/N_{t-1}$ for fixed underlying recruitment intensity.

with the same coefficient prior and covariance structure (Eqs. (13) and (14)):

$$b \sim \text{MVN}(\mu_b, \mathbf{K}) \qquad (13)$$

$$K_{i,j} = \eta^2 \exp(-0.5\,\rho^2 (j-i)^2) \qquad (14)$$

where the response variable Y_t is the number of seedlings in year t, and N_{t-1} is the sample size of reproductive adults in year $t-1$. The model is otherwise similar to the point estimates model, except that we use year-specific intercepts (α_t) to incorporate the Poisson offset (N_{t-1}), rather than a single model intercept as before. We fit the above-described models again, with priors and settings as described in Supplementary Methods section S1.4.

For the stage-specific survival comparison shown in the climate figures, we derived annual stage-specific survival probabilities as column sums of U (survive and transition to any living stage). We then estimated temperature effects for each stage under two matched formulations on the logit scale: an SSD-weighted quasibinomial GLM for point estimates (surv ~ tmp, with weights from the stable stage distribution of each annual U matrix) and a binomial count model for uncertainty propagation (cbind$(n_{\text{surv}}, n_{\text{fail}})$ ~ tmp). Full implementation details are provided in Supplementary Methods sections S1.6 and S1.9.

Analysis 3: Multi-site extension of climate-demography models

To test whether the analysis 2 conclusions generalise across populations, we applied the same paired modelling framework to three *Astragalus scaphoides* populations (Haynes Creek, McDevitt Creek, and Sheep Corral Gulch) (Crone & Lesica, 2004) . For each site, we fit the same two

recruitment-temperature formulations used in analysis 2: a point-estimate model and a sampling-uncertainty model, for both (i) monthly-lag coefficients in the Gaussian-process framework and (ii) a simplified spring-temperature model.

We also fit the same paired stage-specific survival-temperature comparison used in analysis 2, deriving annual stage-specific survival from U-column sums and comparing an SSD-weighted quasibinomial point-estimate model with a binomial count model that propagates sampling uncertainty. This preserves comparable linear predictors across formulations while varying only how uncertainty enters the response model. Full implementation details are given in Supplementary Methods section S1.9.

All analyses were run in R (4.5.3) using RStan (2.32.7), with data handling and plotting in tidyverse packages.

Results

Analysis 1: Comparative analysis of mortality trajectories

We first summarise the overall contribution of sampling uncertainty to observed trait variation using variance-component ratios (Table 1), then ask whether this variation is large enough to alter inference in a specific comparative analysis.

For our parameters of interest, life expectancy and shape, the estimated sampling-to-other variance ratios across population-level MPM entries in analysis 1 were 1.93 and 3.31, respectively (Table 1). Point estimates of life expectancy and shape often deviated from their respective sampling distributions (Fig. 3). For shape, the most extreme positive and negative point estimates tended to have sampling distributions shifted much closer to zero, whereas for mature life expectancy, many point estimates were skewed upward from the median of the sampling distribution. The mismatches between point estimates and sampling distributions usually

411 coincided with a boundary estimate of stage-specific survival (i.e. a point estimate approaching
412 either 0% or 100%). Supplementary analyses suggest that these boundary estimates can skew a
413 point estimate of life expectancy or shape away from the majority of its sampling distribution
414 (see Supplementary Figure S1 and Supplementary Figure S2).

415 Despite the mismatch between point estimates and sampling distributions, accounting for
416 sampling uncertainty in our test of the relationship between life expectancy and shape only
417 moderately affected the overall result (Fig. 4). For the slope parameter β, the posterior
418 distribution from the point-estimate model was centred slightly to the left of zero ($P[\beta > 0] =$
419 0.146), whereas the corresponding posterior from the sampling-uncertainty model was shifted
420 somewhat to the right ($P[\beta > 0] = 0.770$), indicating stronger evidence for a positive relationship
421 between life expectancy and shape.

422 Counterintuitively, there was less posterior uncertainty in β in the sampling-uncertainty model
423 than in the point-estimate model. To see why, consider that a regression slope is harder to
424 estimate precisely when the data are very spread out, because many different slopes could fit the
425 data reasonably well. The point estimates of shape are artificially spread out because boundary-
426 survival estimates drive some of them to extreme values. When those extreme point estimates
427 are replaced by their sampling distributions, which, as Figure 4A shows, tend to cluster much
428 closer to zero, the data are effectively less dispersed, and the slope becomes easier to pin down.

429 *Analysis 2: The impact of weather on demographic traits*

430 Despite the relatively small sample sizes underlying some recruitment estimates (the three
431 smallest sample sizes of reproductive individuals were 8, 12, and 13, respectively), results from
432 the point-estimate model and the sampling-uncertainty model were virtually identical (Fig. 5).
433 Both models identified temperature deviations in monthly lags 7-9 (February-April, prior to the
434 start of the transition interval in July) as having a positive effect on recruitment. If we simplify
435 our model and consider only the relationship between recruitment and mean spring temperature

436 deviations (see Supplementary Methods section S1.6 and Supplementary Table S5), we again find
437 that the point-estimate model is similar to the model incorporating sampling uncertainty (Fig. 5).
438 The estimate of the temperature coefficient β was 8.0% higher, and the 95% interval width for
439 that estimate was 10.9% higher, in the model incorporating sampling uncertainty compared with
440 the point-estimate model. A difference of this magnitude is unlikely to qualitatively change any
441 inferences drawn from a model. In the stage-specific survival panel (Fig. 5C), temperature
442 coefficients were estimable for stages 2 and 3; for stage 1 we show a descriptive open-circle
443 marker at mean survival across years, and for stage 4 (all years at 100% survival) we show a
444 descriptive open-circle marker at survival = 1, both without interval bars. This is analogous to
445 the pattern in Figure 4: once sampling variation in the annual survival estimates is modelled
446 explicitly, part of the apparent between-year spread is reallocated from biological signal to
447 measurement noise, which can yield more precise coefficient estimates.

448 *Analysis 3: Multi-site extension of climate-demography models*

449 Extending the same framework to three *Astragalus scaphoides* populations yielded the same overall
450 pattern: point-estimate and sampling-uncertainty models were closely aligned within site, while
451 differences among sites were more pronounced (Fig. 6). Across sites, we had 9-11 years of
452 annual demographic records, with 8-10 years retained for model fitting after filtering (0-3 years
453 excluded; Supplementary Table S7).

454 For spring-temperature models, posterior medians differed only slightly between formulations
455 (maximum absolute within-site difference: 0.026 on the linear predictor scale), and 95% interval
456 widths changed by only -5.3% to 4.7% across sites (Supplementary Table S8). Monthly-lag
457 coefficient profiles were likewise highly concordant between formulations, with within-site
458 correlations of posterior medians ranging from 0.992 to 0.997 and a maximum lag-specific
459 median difference of 0.042 (Fig. 6). As in analysis 2, these results indicate limited sensitivity of
460 climate-effect inference to transition-rate sampling uncertainty in this setting.

Discussion

When does transition-rate sampling uncertainty materially affect inference from published MPMs?

Sampling uncertainty in the transition rates underlying matrix population models can, in principle, propagate into substantial uncertainty in the demographic traits derived from those models. However, our results show that the impact of sampling uncertainty on inference from published MPMs is strongly trait-dependent. In our analyses, accounting for transition-rate sampling uncertainty moderately affected inference in a comparative analysis of mortality trajectories, but had little impact on a within-species analysis of weather effects on recruitment. It is important to note that the within-species result pertains specifically to an aggregate reproductive transition (seedlings per reproductive adult) rather than to stage-specific survival transitions, which are more commonly affected by boundary estimates. The contrast between analyses 1 and 2 therefore reflects both the type of trait analysed and the type of transition underlying it.

We use "materially affects inference" to mean a difference large enough to change a qualitative conclusion, for instance, by shifting the direction of an estimated effect, moving a credible interval from largely overlapping to largely excluding zero, or substantially altering the rank order of populations. This is a judgment call rather than a formal threshold, and readers with different tolerances for uncertainty may draw the lines differently. This contrast illustrates that ignoring sampling uncertainty does not universally compromise inference from published projection matrices, but that its consequences depend on the traits being analysed and the structure of the underlying models.

For several commonly used integrated demographic metrics, such as population growth rate (λ), generation time, and individual growth rate, sampling uncertainty accounted for only a small fraction of the total variation observed among populations. By contrast, traits related to mortality

trajectories, particularly the shape of the mortality distribution, were far more sensitive: nearly half of the total variation in shape was attributable to sampling uncertainty. In these cases, much of the apparent variation among published MPMs is not distinguishable from statistical noise. This result helps explain why incorporating sampling uncertainty shifted inference in the senescence analysis but had little effect in the climate-recruitment analysis, where the response variable was more directly linked to observed counts and less dependent on long-term survivorship.

Why are some MPM-derived traits particularly sensitive to sampling uncertainty, and what are the practical implications?

The sensitivity of mortality-trajectory traits has a single underlying cause: life expectancy and shape are inferred via age-from-stage methods, which project a cohort forward through repeated matrix multiplication. Errors in late-stage survival are therefore not simply carried forward but compounded across projection steps, amplifying small transition-rate uncertainties into large uncertainties in long-term survivorship. Integrated metrics like population growth rate are insulated from this because they reflect a weighted average over all transitions simultaneously, where errors tend to partially cancel.

Several structural features of published matrices exacerbate this. In our analysis 1 set ($n = 68$ population-level matrices), 47% (32/68) contain only a single reproductive stage class, 69% (47/68) reach their quasi-stable distribution in less than one life expectancy, and 46% (31/68) contain at least one stage-specific survival estimate of exactly 100%. These are not rare edge cases; they are routine features of published matrices that systematically displace derived trait estimates from the centre of their sampling distributions.

Practical implications for users of compiled demographic databases

These structural constraints have practical implications. Analyses based on highly aggregated demographic metrics, such as population growth rate, mean vital rates, or generation time, are often robust to sampling uncertainty and may not require explicit uncertainty modelling. Analyses of ageing, longevity, or mortality trajectories are considerably more sensitive and should be treated with caution unless sampling uncertainty is explicitly incorporated.

Analyses warrant caution when: any stage has survival >0.95 or <0.05, or is estimated from fewer than 20 individuals; the matrix has only a single reproductive stage class; or the time to quasi-stable distribution is less than one life expectancy. Conversely, analyses are likely robust when survival estimates are well away from boundaries, key transitions are estimated from >50 individuals, and the focal metric is highly integrated (e.g. population growth rate, generation time). The absence of a detectable uncertainty effect (as in our climate-recruitment analysis) should not be taken as general evidence that propagation is unnecessary; robustness is trait- and context-specific.

Sampling uncertainty versus demographic stochasticity

It is important to emphasise that our analysis of sampling uncertainty is distinct from demographic stochasticity, a distinction that is sometimes blurred in the literature (Kendall 1998). In the current study, we assume that the parameter of interest is the population mean of a demographic trait and focus exclusively on uncertainty arising from finite sampling of that mean. In addition, individuals within a population are likely to exhibit genuine variation around the population mean in demographic rates, giving rise to demographic stochasticity. Both sources of uncertainty can have important implications for applications such as population viability analyses, where failing to account for either demographic stochasticity or sampling uncertainty can lead to biased estimates of extinction risk (Kendall and Fox 2002, McGowan et al. 2011).

Distinguishing between these sources of uncertainty is therefore essential for appropriate interpretation.

Data limitations and reporting considerations

Incorporating transition-rate sampling uncertainty into analyses of published MPMs remains challenging, primarily because the data required to reconstruct sampling distributions are rarely reported. Of the 91 source publications we initially targeted, only a small subset provided sufficient information to model uncertainty in survival or reproductive transitions. Improved reporting of transition-specific sample sizes or standard errors, particularly on the scale of the linear predictor, would greatly enhance future researchers' ability to assess robustness and propagate uncertainty where necessary (see Supplementary Methods section S1.7 for detailed recommendations). At the same time, the absence of a single, universally "correct" approach to modelling transition rates should not deter progress. Even partial information can be sufficient to identify cases where inference is likely to be robust or fragile, and recognising the limits of inference is often as important as refining point estimates. Viewed in this light, accounting for sampling uncertainty is not simply a technical exercise but a means of understanding when demographic inference from compiled databases can be trusted and when it should be treated with caution.

Conclusions

Our analyses show that the consequences of transition-rate sampling uncertainty in published matrix population models are highly trait-dependent. For many commonly used integrated demographic metrics, such as population growth rate and generation time, sampling uncertainty accounted for only a small fraction of total variation, suggesting that inference from published MPMs is often robust for these traits. By contrast, parameters related to mortality trajectories, including life expectancy and, especially, the shape of the mortality distribution, were substantially more sensitive to sampling uncertainty. In these cases, a large proportion of

apparent variation among published matrices is indistinguishable from statistical noise, and point estimates can be systematically biased by boundary estimates of stage-specific survival.

These results indicate that accounting for sampling uncertainty will not universally alter conclusions drawn from analyses of published MPMs, but that its importance depends critically on the demographic traits being analysed and on features of model structure and data availability. Although our study examined only a subset of MPM-derived parameters and a limited fraction of the matrices available in COMPADRE, it highlights specific conditions under which inference is likely to be fragile and provides practical guidance for assessing robustness in comparative and time-series analyses.

More broadly, the growing availability of large, compiled demographic databases presents both new opportunities and new challenges. The data underlying these databases were collected for diverse purposes, using heterogeneous sampling designs and statistical approaches, resulting in variation not only in sampling uncertainty but also in underlying assumptions and context. Recognising and accounting for these limitations through improved reporting in primary studies and careful, trait-specific interpretation in secondary analyses will be essential to ensure that comparative demography based on published projection matrices yields reliable and biologically meaningful inferences.

Acknowledgements

We are indebted to the COMPADRE data digitisation team and management committee for their work in developing the COMPADRE Plant Matrix Database. We thank the original study authors who shared additional sample-size information and supporting materials, which enabled the inclusion of those matrices in our analyses. We are especially grateful to Patrick Barks for substantial preparatory work and early analytical contributions to this project. This work was supported by a grant from the Independent Research Fund Denmark (grant 6108-00467B).

Author contributions

ORJ conceived and designed the study, curated data from the COMPADRE database and data provided by authors of papers selected as case studies, conducted the analysis, and wrote the first draft of the manuscript. EGS contributed to conceptualization and interpretation of results, and reviewed and edited the manuscript. Both authors approved the final version for submission.

Conflict of interest

The authors declare no conflict of interest.

Data availability

Data and code required to reproduce our analyses are archived on Zenodo: https://doi.org/10.5281/zenodo.19474729.

Supplementary Materials

The supplementary materials include the following items:

- **Supplementary Methods S1.1**: Sampling-distribution workflow used for each MPM.
- **Supplementary Methods S1.2**: Age-from-stage derivation, truncation, and shape metric.
- **Supplementary Methods S1.3**: Pooled and mean MPM handling.
- **Supplementary Methods S1.4**: Bayesian model priors and fitting settings.
- **Supplementary Methods S1.5**: Variance-component summary (sampling-to-other ratio).
- **Supplementary Methods S1.6**: Simplified spring-temperature model (analysis 2).
- **Supplementary Methods S1.7**: Reporting recommendations for future MPM studies.

- **Supplementary Methods S1.8**: Species identities in analysis 1.
- **Supplementary Methods S1.9**: Multi-site extension for analysis 3 (*Astragalus scaphoides*).
- **Supplementary Results S2.1**: Sensitivity to point-estimate weighting choice (no weights vs SSD weights).
- **Table S1**: Single-MPM derived-parameter summary for the focal *Agrimonia eupatoria* example.
- **Table S2**: Mean-MPM derived-parameter summary for the focal *Agrimonia eupatoria* example (population B).
- **Table S3**: Analysis 1 posterior summary for the slope parameter (β) in the life expectancy-shape model.
- **Table S4**: Analysis 2 Gaussian-process regression coefficients (monthly lags) for recruitment responses to temperature anomalies.
- **Table S5**: Analysis 2 posterior summary for the spring-temperature coefficient.
- **Table S6**: Primary studies represented in the analysis subset, as identified in COMPADRE.
- **Table S7**: Analysis 3 site coverage and spring-temperature effect summaries for *Astragalus scaphoides*.
- **Table S8**: Analysis 3 posterior summary for the spring-temperature coefficient by site and model formulation.
- **Table S9**: Analysis 2 stage-specific survival-temperature coefficients under no weights and SSD weights.
- **Table S10**: Analysis 3 stage-specific survival-temperature coefficients under no weights and SSD weights.
- **Figure S1**: Boundary-estimate diagnostic.

- **Figure S2**: Illustration of survivorship trajectories under boundary survival transitions.

References

Adler, P. B., Salguero-Gómez, R., Compagnoni, A., Hsu, J. S., Ray-Mukherjee, J., Mbeau-Ache, C., and Franco, M. (2014) Functional traits explain variation in plant life history strategies. *Proceedings of the National Academy of Sciences*, 111, 740-745. https://doi.org/10.1073/pnas.1315179111

Baudisch, A. (2011) The pace and shape of ageing. *Methods in Ecology and Evolution*, 2, 375-382. https://doi.org/10.1111/j.2041-210X.2010.00087.x

Baudisch, A., Salguero-Gómez, R., Jones, O. R., Wrycza, T., Mbeau-Ache, C., Franco, M., and Colchero, F. (2013) The pace and shape of senescence in angiosperms. *Journal of Ecology*, 101, 596-606. https://doi.org/10.1111/1365-2745.12084

Biggs, R., Carpenter, S. R., and Brock, W. A. (2009) Spurious certainty: how ignoring measurement error and environmental heterogeneity may contribute to environmental controversies. *BioScience*, 59, 65-76. https://doi.org/10.1525/bio.2009.59.1.10

Caswell, H. (2001) *Matrix population models: construction, analysis, and interpretation*, 2nd ed. Sinauer, Sunderland, MA.

Cochran, M. E., and Ellner, S. (1992) Simple Methods for Calculating age-based life history parameters for stage-structured populations. *Ecological Monographs*, 62, 345-364. https://doi.org/10.2307/2937115

Coutts, S. R., Salguero-Gómez, R., Csergő, A. M., and Buckley, Y. M. (2016) Extrapolating demography with climate, proximity and phylogeny: approach with caution. *Ecology Letters*, 19, 1429-1438. https://doi.org/10.1111/ele.12691

Crone, E.E. and Lesica, P. (2004) Causes of synchronous flowering in *Astragalus scaphoides*, an iteroparous perennial plant. *Ecology*, 85: 1944-1954. https://doi.org/10.1890/03-0256

650 Csergő, A. M., Salguero-Gómez, R., Broennimann, O., Coutts, S. R., Guisan, A., Angert, A. L.,
651 Welk, E., Stott, I., Enquist, B. J., McGill, B., Svenning, J. C., Violle, C., and Buckley, Y. M.
652 (2017) Less favourable climates constrain demographic strategies in plants. *Ecology Letters*, 20,
653 969-980. https://doi.org/10.1111/ele.12794

654 Daly, C., Halbleib, M., Smith, J. I., Gibson, W. P., Doggett, M. K., Taylor, G. H., Curtis, J., and
655 Pasteris, P. A. (2008) Physiographically sensitive mapping of climatological temperature and
656 precipitation across the conterminous United States. *International Journal of Climatology*, 28, 2031-
657 2064. https://doi.org/10.1002/joc.1688

658 de Magalhães, J. P., and Costa, J. (2009) A database of vertebrate longevity records and their
659 relation to other life-history traits. *Journal of Evolutionary Biology*, 22, 1770-1774.
660 https://doi.org/10.1111/j.1420-9101.2009.01783.x

661 Ellis, M. M., Williams, J. L., Lesica, P., Bell, T. J., Bierzychudek, P., Bowles, M., Crone, E. E.,
662 Doak, D. F., Ehrlén, J., Ellis-Adam, A., McEachern, K., Ganesan, R., Latham, P., Luijten, S.,
663 Kaye, T. N., Knight, T. M., Menges, E. S., Morris, W. F., den Nijs, H., Oostermeijer, G.,
664 Quintana-Ascencio, P. F., Shelly, J. S., Stanley, A., Thorpe, A., Ticktin, T., Valverde, T., Weekley,
665 C. W. (2012) Matrix population models from 20 studies of perennial plant populations. *Ecology*,
666 93, 951-951. https://doi.org/10.1890/11-1052.1

667 Franco, M., and Silvertown, J. (1996) Life history variation in plants: an exploration of the fast-
668 slow continuum hypothesis. *Philosophical Transactions of the Royal Society of London B*, 351, 1341-
669 1348. https://doi.org/10.1098/rstb.1996.0117

670 Fristoe, T. S., Iwaniuk, A. N., and Botero, C. A. (2017) Big brains stabilize populations and
671 facilitate colonization of variable habitats in birds. *Nature Ecology & Evolution*, 1, 1706.
672 https://doi.org/10.1038/s41559-017-0316-2

673 Garratt, M., Gaillard, J.-M., Brooks, R. C., and Lemaître, J.-F. (2013) Diversification of the
674 eutherian placenta is associated with changes in the pace of life. *Proceedings of the National Academy*
675 *of Sciences*, 110, 7760-7765. https://doi.org/10.1073/pnas.1305018110

676 Healy, K., Guillerme, T., Finlay, S., Kane, A., Kelly, S. B. A., McClean, D., Kelly, D. J.,
677 Donohue, I., Jackson, A. L., and Cooper, N. (2014) Ecology and mode-of-life explain lifespan
678 variation in birds and mammals. *Proceedings of the Royal Society B: Biological Sciences*, 281, 20140298.
679 https://doi.org/10.1098/rspb.2014.0298

680 Healy, K., Ezard, T. H. G., Jones, O. R., Salguero-Gómez, R., and Buckley, Y. M. (2019) Animal
681 life history is shaped by the pace of life and the distribution of age-specific mortality and
682 reproduction. *Nature Ecology & Evolution*, 3, 1217-1224. https://doi.org/10.1038/s41559-019-
683 0938-7

684 Horvitz, C. C., and Tuljapurkar, S. (2008) Stage dynamics, period survival, and mortality plateaus.
685 *The American Naturalist*, 172, 203-215. https://doi.org/10.1086/589453

686 Jones, K. E., Bielby, J., Cardillo, M., Fritz, S. A., O'Dell, J., Orme, C. D. L., Safi, K., Sechrest,
687 W., Boakes, E. H., Carbone, C., Connolly, C., Cutts, M. J., Foster, J. K., Grenyer, R., Habib, M.,
688 Plaster, C. A., Price, S. A., Rigby, E. A., Rist, J., Teacher, A., Bininda-Emonds, O. R. P.,
689 Gittleman, J. L., Mace, G. M., and Purvis, A. (2009) PanTHERIA: a species-level database of life
690 history, ecology, and geography of extant and recently extinct mammals. *Ecology*, 90, 2648-2648.
691 https://doi.org/10.1890/08-1494.1

692 Jones, O. R., Scheuerlein, A., Salguero-Gómez, R., Camarda, C. G., Schaible, R., Casper, B. B.,
693 Dahlgren, J. P., Ehrlén, J., García, M. B., Menges, E. S., Quintana-Ascencio, P. F., Caswell, H.,
694 Baudisch, A., and Vaupel, J. W. (2014) Diversity of ageing across the tree of life. *Nature*, 505,
695 169-173. https://doi.org/10.1038/nature12789

696 Kendall, B. E. (1998) Estimating the magnitude of environmental stochasticity in survivorship
697 data. *Ecological Applications*, 8, 184-193. https://doi.org/10.1890/1051-
698 0761(1998)008[0184:ETMOES]2.0.CO;2

699 Kendall, B. E., and Fox, G. A. (2002) Variation among individuals and reduced demographic
700 stochasticity. *Conservation Biology*, 16, 109-116. https://doi.org/10.1046/j.1523-1739.2002.00036.x

701 Kiviniemi, K. (2002) Population dynamics of *Agrimonia eupatoria* and *Geum rivale*, two perennial
702 grassland species. *Plant Ecology*, 159, 153-169. https://doi.org/10.1023/A:1015506019670

703 Lesica, P., and Crone, E. E. (2007) Causes and consequences of prolonged dormancy for an
704 iteroparous geophyte, *Silene spaldingii*. *Journal of Ecology*, 95, 1360-1369.
705 https://doi.org/10.1111/j.1365-2745.2007.01291.x

706 McDonald, J. L., Franco, M., Townley, S., Ezard, T. H., Jelbert, K., and Hodgson, D. J. (2017)
707 Divergent demographic strategies of plants in variable environments. *Nature Ecology & Evolution*,
708 1, 0029. https://doi.org/10.1038/s41559-016-0029

709 McElreath, R. (2020) Statistical rethinking: A Bayesian course with examples in R and Stan, 2nd
710 ed. Chapman and Hall/CRC. https://doi.org/10.1201/9780429029608

711 McGowan, C. P., Runge, M. C., and Larson, M. A. (2011) Incorporating parametric uncertainty
712 into population viability analysis models. *Biological Conservation*, 144, 1400-1408.
713 https://doi.org/10.1016/j.biocon.2011.01.005

714 Myhrvold, N. P., Baldridge, E., Chan, B., Sivam, D., Freeman, D. L., and Ernest, S. M. (2015)
715 An amniote life-history database to perform comparative analyses with birds, mammals, and
716 reptiles. *Ecology*, 96, 3109-3109. https://doi.org/10.1890/15-0846R.1

717 PRISM Group, Oregon State University (2026) PRISM Climate Data.
718 https://prism.oregonstate.edu. Data created 04 Feb 2026, accessed 28 Feb 2026.

719 Salguero-Gómez, R., Jones, O. R., Archer, C. R., Buckley, Y. M., Che-Castaldo, J., Caswell, H.,
720 Hodgson, D., Scheuerlein, A., Conde, D. A., Brinks, E., de Buhr, H., Farack, C., Gottschalk, F.,
721 Hartmann, A., Henning, A., Hoppe, G., Römer, G., Runge, J., Ruoff, T., Wille, J., Zeh, S.,
722 Davison, R., Vieregg, D., Baudisch, A., Altwegg, R., Colchero, F., Dong, M., de Kroon, H.,
723 Lebreton, J.-D., Metcalf, C. J. E., Neel, M. M., Parker, I. M., Takada, T., Valverde, T., Vélez-
724 Espino, L. A., Wardle, G. M., Franco, M., and Vaupel, J. W. (2015) The COMPADRE Plant
725 Matrix Database: an open online repository for plant demography. *Journal of Ecology*, 103, 202-
726 218. https://doi.org/10.1111/1365-2745.12334

727 Salguero-Gómez, R., Jones, O. R., Archer, C. R., Bein, C., de Buhr, H., Farack, C., Gottschalk,
728 F., Hartmann, A., Henning, A., Hoppe, G., Romer, G., Ruoff, T., Sommer, V., Wille, J., Voigt, J.,
729 Zeh, S., Vieregg, D., Buckley, Y. M., Che-Castaldo, J., Hodgson, D., Scheuerlein, A., Caswell, H.,
730 and Vaupel, J. W. (2016a) COMADRE: a global data base of animal demography. *Journal of*
731 *Animal Ecology*, 85, 371-384. https://doi.org/10.1111/1365-2656.12482

732 Salguero-Gómez, R., Jones, O. R., Jongejans, E., Blomberg, S. P., Hodgson, D. J., Mbeau-Ache,
733 C., Zuidema, P. A., de Kroon, H., and Buckley, Y. M. (2016b) Fast–slow continuum and
734 reproductive strategies structure plant life-history variation worldwide. *Proceedings of the National*
735 *Academy of Sciences*, 113, 230-235. https://doi.org/10.1073/pnas.1506215112

736 Baudisch, A., and Stott, I. (2019) A pace and shape perspective on fertility. *Methods in Ecology and*
737 *Evolution*, 10, 1941-1951. https://doi.org/10.1111/2041-210X.13289

738 Carpenter, B., Gelman, A., Hoffman, M. D., Lee, D., Goodrich, B., Betancourt, M., Brubaker,
739 M., Guo, J., Li, P., and Riddell, A. (2017) Stan: A probabilistic programming language. *Journal of*
740 *Statistical Software*, 76, 1-32. https://doi.org/10.18637/jss.v076.i01

741 Simmonds, E. G., and Jones, O. R. (2024) Uncertainty propagation in matrix population models:
742 gaps, importance and guidelines. *Methods in Ecology and Evolution*, 15, 427-438.
743 https://doi.org/10.1111/2041-210X.14276

744 Stan Development Team (2025) RStan: the R interface to Stan. R package version 2.32.7.
745 https://mc-stan.org/ https://doi.org/10.32614/CRAN.package.rstan

746 Teller, B. J., Adler, P. B., Edwards, C. B., Hooker, G., and Ellner, S. P. (2016) Linking
747 demography with drivers: climate and competition. *Methods in Ecology and Evolution*, 7, 171-183.
748 https://doi.org/10.1111/2041-210X.12486

749 Wrycza, T. F., Missov, T. I., and Baudisch, A. (2015) Quantifying the shape of aging. *PLOS*
750 *ONE*, 10, e0119163. https://doi.org/10.1371/journal.pone.0119163

751

Tables

Table 1: Sampling-to-other variance ratios for key demographic parameters in analysis 1. Ratios greater than 1 indicate that variance attributable to transition-rate sampling uncertainty exceeds residual biological variance across population-level entries (including both among-population and among-species variation). The table shows that this ratio is highest for shape, intermediate for life expectancy, and lowest for log population growth rate.

Parameter	Sampling:other variance ratio
Shape	3.31
Life expectancy	1.93
Log population growth rate	1.01
Damping ratio	1.12
Generation time	1.63
Probability of reaching maturity	1.62

Figures

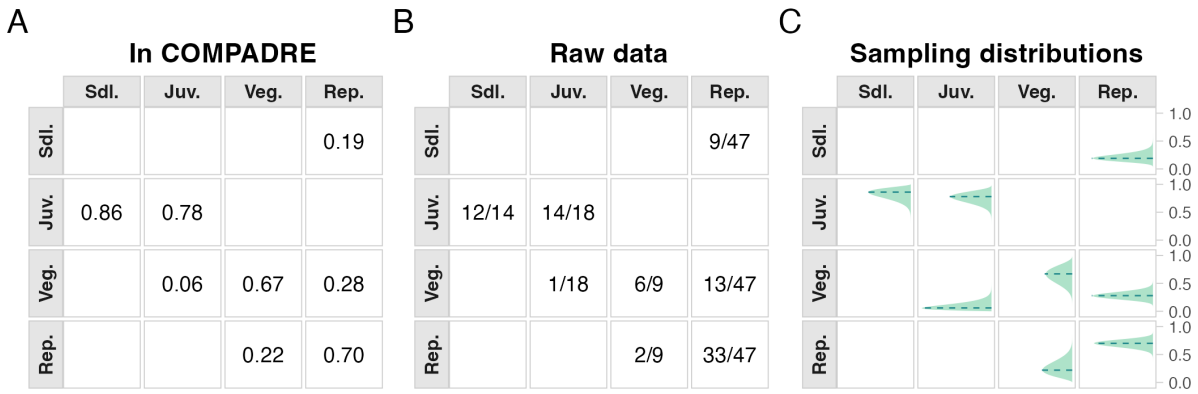

Figure 1: Sampling distributions of transition rates for the focal single-MPM example (Agrimonia eupatoria, population B), showing transition rates as reported in COMPADRE (A), the underlying transition counts used for estimation (B), and bootstrap-based sampling distributions (C). In panel C, green density ribbons show transition-rate sampling distributions, red dashed vertical lines show point estimates, and grey dotted vertical lines show posterior medians. Transition rates are probabilities (bounded 0-1). Together, these panels show that several matrix elements are weakly estimated from finite samples.

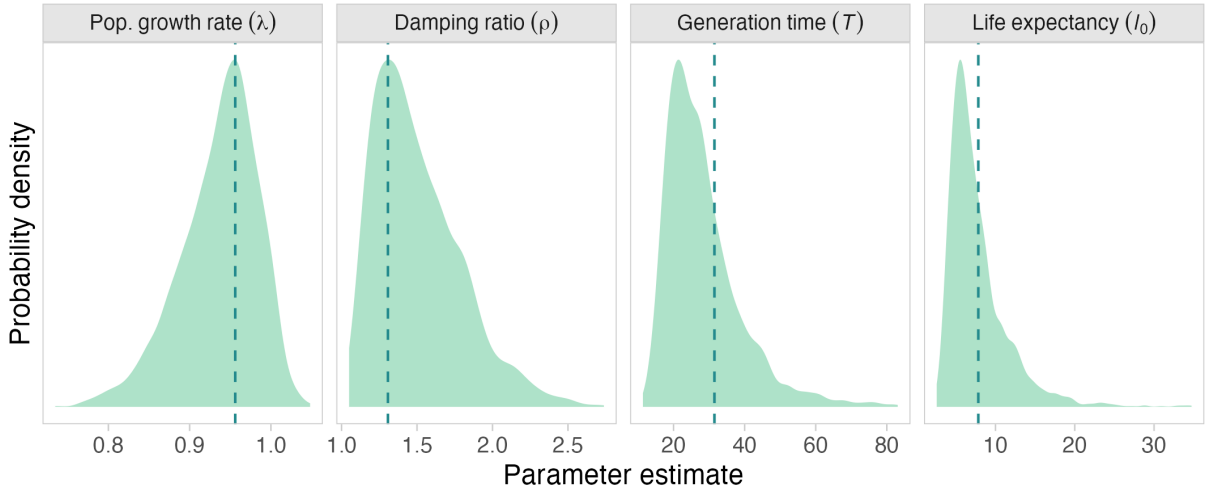

767

768 *Figure 2: Sampling distributions of demographic quantities derived from the focal single MPM, including*

769 *population growth rate (λ), damping ratio (ρ), generation time (T), and life expectancy (l_0). Orange density*

770 *ribbons show derived-quantity sampling distributions; red dashed vertical lines show point estimates; grey dotted*

771 *vertical lines show posterior medians. Quantities are shown on their natural scales (T and l_0 are in years).*

772 *Uncertainty in transition rates propagates to substantial uncertainty in these derived parameters, with the largest*

773 *spread in quantities that depend on long-term survivorship and reproduction.*

774

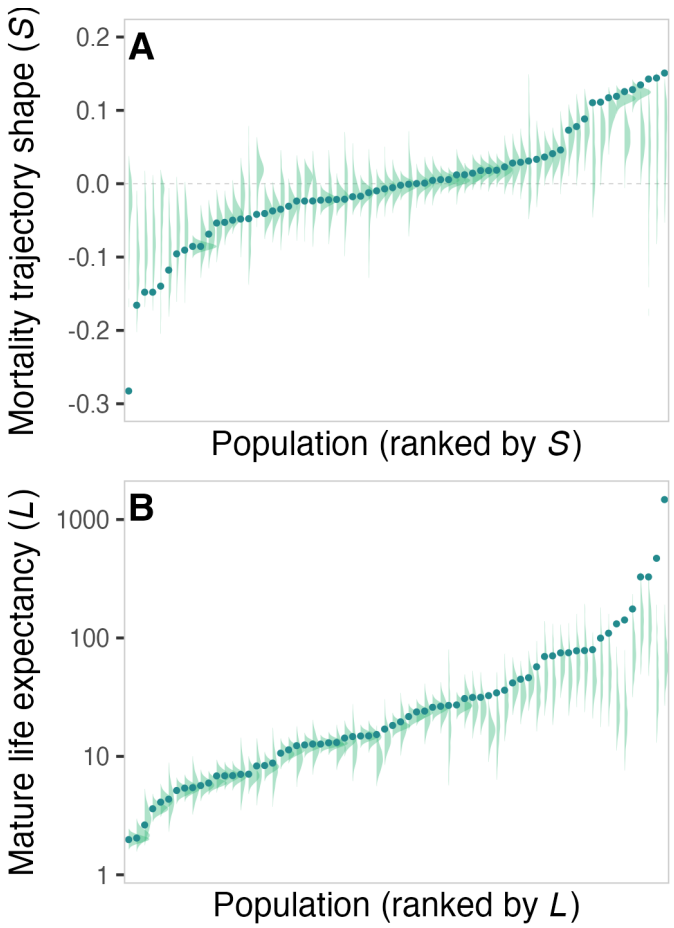

775

776 *Figure 3: Analysis 1 comparison of point estimates versus sampling-distribution summaries for population-level*
777 *life expectancy and shape. Panel A shows mortality-trajectory shape, and panel B shows mature life expectancy*
778 *(years). Purple distributions/points correspond to estimates from matrix point estimates, and green*
779 *distributions/points correspond to uncertainty-aware summaries from transition-rate sampling distributions. The*
780 *figure shows systematic shifts and shrinkage in extreme values when sampling uncertainty is propagated.*

781

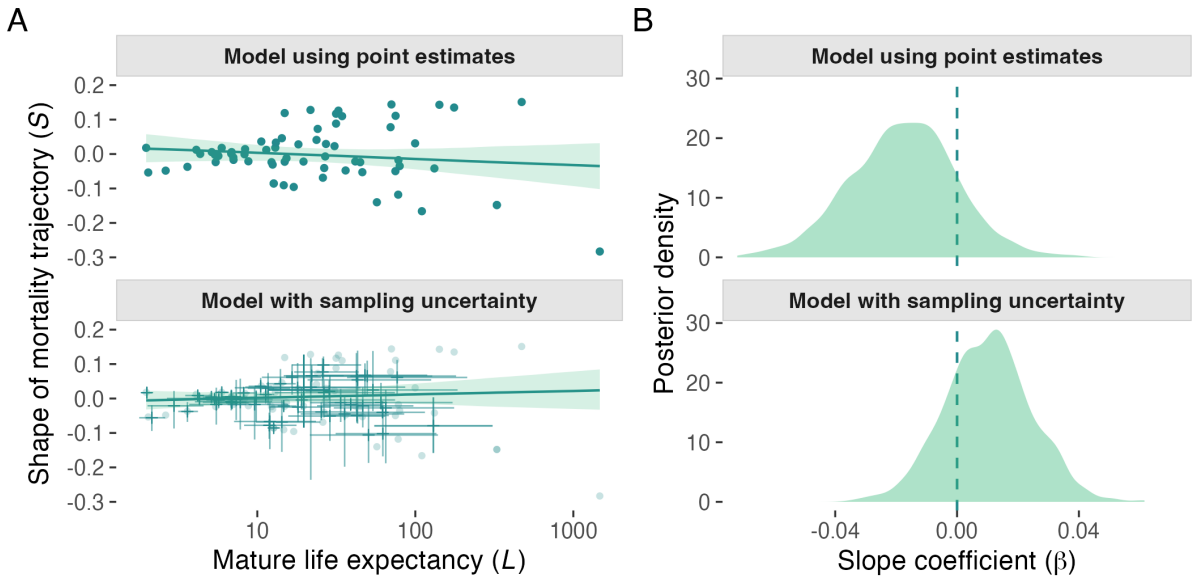

782

783 *Figure 4: Analysis 1 relationship between life expectancy and shape under models with and without sampling*
784 *uncertainty propagation. In panel A, purple points/line/ribbon show the model using point estimates. Green*
785 *crosses/line/ribbon show the uncertainty-aware model; crosses are centred on sampling-distribution medians with*
786 *horizontal and vertical bars showing 95% intervals. The displacement between faint reference points and crosses*
787 *indicates that propagated sampling distributions can shift central tendency away from point estimates, consistent*
788 *with the offsets between dashed lines and density peaks in Figure 3. Axes are mature life expectancy (years, log*
789 *scale) and mortality-trajectory shape. Panel B shows posterior densities for the slope parameter β (unit change in*
790 *shape per unit change in log life expectancy). This figure shows that accounting for sampling uncertainty shifts*
791 *posterior support towards a positive association.*

792

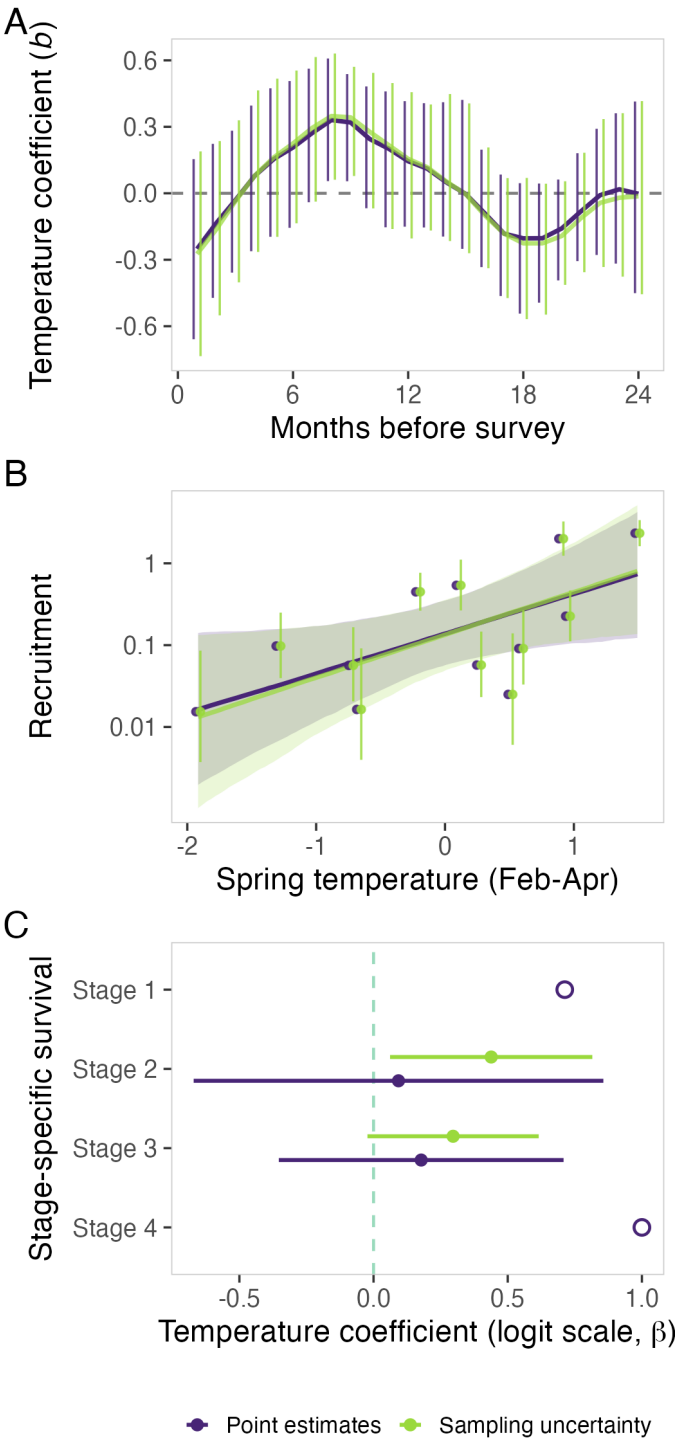

793

794 *Figure 5: Analysis 2 climate effects on recruitment and stage-specific survival in Silene spaldingii. Panels A-B*

795 *show monthly-lag and spring-temperature recruitment models for point-estimate (purple) and uncertainty-aware*

796 *(green) formulations, with similar posterior coefficient estimates and interval widths. In panel A, y-values are*

797 *temperature coefficients b for monthly temperature deviations (months before survey on the x-axis). In panel B,*

recruitment is seedlings per reproductive plant and spring temperature is February-April temperature deviation. Panel C shows stage-specific survival-temperature coefficients on the logit scale (beta) where estimable (stages 2-3). Open circles in panel C are descriptive markers without interval bars for non-estimable stages: stage 1 shows mean survival across years, and stage 4 shows survival = 1 (100% survival in all usable years).

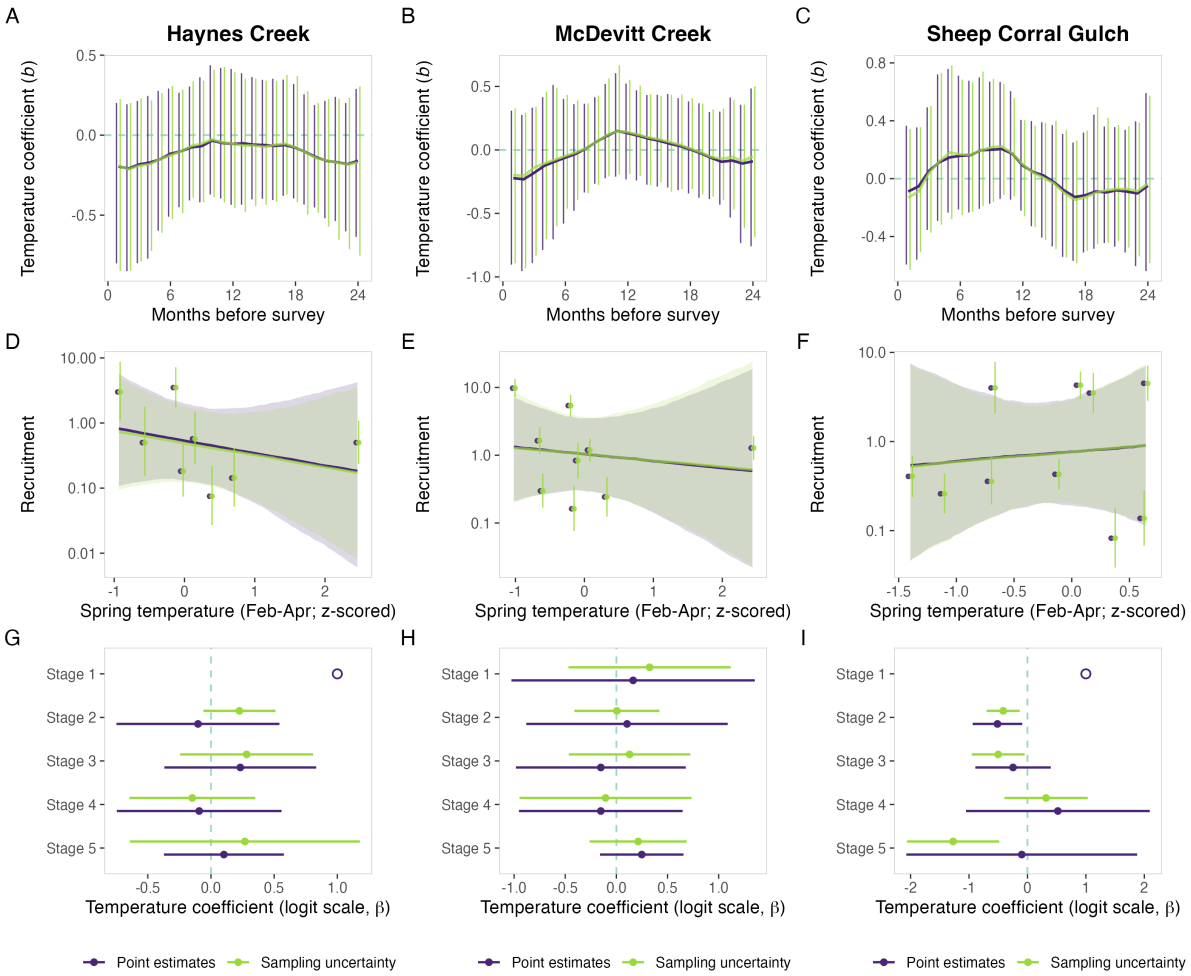

803

804 *Figure 6: Analysis 3 multisite climate-demography comparison for Astragalus scaphoides. Panel A (Haynes*
805 *Creek), panel B (McDevitt Creek), and panel C (Sheep Corral Gulch) each show monthly-lag temperature*
806 *coefficients, recruitment-temperature fits, and stage-specific survival-temperature coefficients for point-estimate*
807 *(purple) and uncertainty-aware (green) formulations. Recruitment is seedlings per reproductive plant, and stage-*
808 *specific survival coefficients are on the logit scale (β). Across sites, the two formulations remain closely aligned,*
809 *showing that among-site ecological differences are larger than differences induced by uncertainty propagation.*

810

Supplementary Methods

S1.1 Sampling-distribution workflow used for each MPM

For each focal matrix population model (MPM), we reconstructed transition-level sampling distributions from reported transition counts (or equivalent sample-size information). We then generated 2,000 parametric bootstrap draws per MPM by sampling each transition from its likelihood (multinomial for survival/growth/retrogression transitions and Poisson for recruitment transitions), rebuilding the full MPM for each draw, and recalculating each derived demographic quantity from that draw. We treated structural zeros (biologically impossible transitions) as fixed zeros in all draws, and treated sampling zeros (possible but unobserved transitions) as uncertain parameters under the same likelihood models used for non-zero transitions. When a recovered stage-specific sample size was zero, we retained the published point-estimate transition column unchanged in all bootstrap draws rather than treating it as structurally fixed at zero; this preserves the published matrix while acknowledging that no additional sampling variance can be propagated for that column.

This produced a sampling distribution for each derived quantity used downstream (e.g. life expectancy, shape, log population growth rate). Point estimates in the manuscript correspond to values derived directly from the reported matrix entries; uncertainty-aware summaries correspond to moments of these bootstrap distributions.

S1.2 Age-from-stage derivation, truncation, and shape metric

Life expectancy and shape were derived from survivorship trajectories obtained using age-from-stage methods, starting from the first reproductive stage. Shape was calculated using the pace-shape framework metric (Baudisch and Stott 2019). Because stage-based survivorship can converge to an artefactual mortality plateau, shape was calculated on truncated trajectories up to quasi-stable convergence (distance threshold 1%).

S1.3 Pooled and mean MPM handling

Analysis 1 used one population-level MPM per population. Where a pooled population MPM was available, it was used; otherwise, a mean population MPM was used; if neither was available, a population-level matrix was constructed as the element-wise mean of the available annual individual MPMs. When COMPADRE included both site-specific population rows and aggregate rows that combined multiple populations, only the site-specific population rows were retained, so that each population contributed a single analysis unit. For uncertainty propagation in pooled or mean matrices, stage-specific sample sizes were pooled across years before bootstrap simulation. This captures within-year sampling variation but does not fully represent between-year process variation, so the resulting uncertainty should be interpreted conservatively.

S1.4 Bayesian model priors and fitting settings

Stan models and priors are defined in `models/*.stan`. For the two main analyses:

- Analysis 1 models use weakly informative normal priors for location/slope terms and normal priors for scale terms (see `models/regress_hier.stan` and `models/regress_hier_error.stan`).
- Analysis 2 uses two models with Gaussian-process regression forms and normal priors on GP hyperparameters and coefficients (see `models/movbeta_gprc.stan` and `models/movbeta_gprc_err.stan`).
- Analysis 3 uses the same Gaussian-process recruitment model pair as analysis 2 (`models/movbeta_gprc.stan` and `models/movbeta_gprc_err.stan`) together with a simpler spring-temperature regression pair using weakly informative normal priors on regression coefficients and scale terms (`models/regress.stan` and `models/regress_log_err.stan`).

Fitting settings used in scripts:

- Analysis 1 (`scripts/S07_case_study_1_analysis.R`): `chains = 2`, `iter = 4000`, `warmup = 2000-3000`, `seed = 5654`.
- Analysis 2 (`scripts/S12_case_study_2.R`): `iter = 5000` for key models, `seed = 5654`, with additional control settings for GP fits.
- Analysis 3 (`scripts/S14_case_study_3_astragalus.R`): `iter = 5000`, `seed = 5654`, using the same GP control settings as analysis 2 for recruitment models and matched regression settings for the simplified spring-temperature models.

S1.5 Variance-component summary (sampling-to-other ratio)

For each parameter, the total observed variance was partitioned into:

- sampling component: mean within-MPM sampling variance from bootstrap draws;
- residual component: remaining variance among populations/species.

The reported summary is Eq. (15):

$$\text{ratio} = \frac{v_{\text{sampling}}}{v_{\text{residual}}} \qquad (15)$$

Ratios above 1 indicate that sampling uncertainty exceeds residual biological variation for that parameter.

S1.6 Simplified spring-temperature model (analysis 2)

In addition to the monthly-lagged GP model, we fit a simplified spring summary model with mean spring temperature deviation as the predictor, under both point-estimate and uncertainty-aware formulations. The contrasts reported in the manuscript use posterior medians and 95% interval widths from these paired models.

For the stage-specific survival panel in analysis 2 (Fig. 5C), we derived annual stage-specific survival as the column sums of the U matrix for each year and stage, then compared two logit-

scale models per stage: (i) a stable-stage distribution (SSD)-weighted quasibinomial point-estimate model, surv ~ tmp, where weights are the stable stage distribution from each annual U matrix; and (ii) a binomial count model, cbind$(n_{\text{surv}}, n_{\text{fail}}) \sim$ tmp, where n_{surv} and n_{fail} are survived and non-survived counts implied by stage sample size and U-column survival probability.

S1.7 Reporting recommendations for future MPM studies

To support uncertainty propagation in secondary analyses, primary studies should report (at a minimum):

- transition-level sample sizes for each matrix element (or reconstructable transition count tables);
- clear identification of pooled/mean matrices and pooling rules;
- uncertainty estimates on model-appropriate scales (e.g. linear predictor where relevant);
- explicit projection interval, stage definitions, and treatment filters used to derive published matrices.

These items are usually sufficient for parametric uncertainty reconstruction in compiled databases.

S1.8 Study and species identities in analysis 1

Analysis 1 used a subset of the full compiled dataset: 68 population-level entries representing 25 species. Study-level and species-level identities (including COMPADRE `SpeciesAuthor` labels) are provided in Table S6.

S1.9 Multi-site extension for analysis 3 (Astragalus scaphoides)

To evaluate whether inference robustness in analysis 2 generalised across populations, we repeated the same paired modelling framework for all available *Astragalus scaphoides* sites with

sufficient annual coverage. For each site, we fit (i) a point-estimate model and (ii) a sampling-uncertainty model for recruitment-temperature relationships, using both the monthly-lag Gaussian-process specification and the simplified spring-temperature specification. We then compared posterior medians and 95% intervals between model formulations within site. This design isolates the contribution of uncertainty propagation while preserving site-specific ecological context.

For stage-specific survival in analysis 3, we used the same matched pair as in analysis 2: an SSD-weighted quasibinomial point-estimate model (surv ~ tmp, weights from the stable stage distribution of each annual U matrix) and a binomial count model (cbind$(n_{\text{surv}}, n_{\text{fail}})$ ~ tmp). This keeps the linear predictor and response scale aligned across formulations, differing only in whether survival is treated as a plug-in proportion or as counts with explicit sampling uncertainty.

For sensitivity analyses intended to mimic database-only use (no access to true stage sample sizes), we re-fit stage-specific point-estimate models under two alternatives: (i) no weighting and (ii) SSD weighting derived from each annual U matrix.

Supplementary Results

S2.1 Sensitivity to point-estimate weighting choice

Across estimable stages in analysis 2, switching from no weighting to SSD weighting changed temperature-coefficient medians by at most 0.142 on the logit scale, with interval widths changing by -0.045 to 0.614 (Table S9).

Across estimable site-stage combinations in analysis 3, the corresponding maximum absolute median shift was 0.912, and interval-width differences ranged from -0.512 to 1.526 (Table S10).

These sensitivity checks show how weighting assumptions alter point-estimate uncertainty when true stage sample sizes are unavailable.

Supplementary Tables

Table S1. Single-MPM derived-parameter summary for the focal *Agrimonia eupatoria* example. Reported values are point estimates and uncertainty intervals from parametric bootstrap sampling distributions, showing substantial uncertainty for several derived demographic quantities.

Parameter	Median	Lower 95%	Upper 95%	Point estimate
Pop. growth rate (λ)	0.943	0.826	1.010	0.956
Damping ratio (ρ)	1.440	1.110	2.200	1.310
Reproductive value (vegetative stage)	2.800	0.803	15.000	
Elasticity	0.345	0.145	0.558	
Generation time (*T*)	25.900	15.300	58.100	31.500
Life expectancy (l_0)	6.650	3.600	17.900	7.840

Table S2. Mean-MPM derived-parameter summary for the focal *Agrimonia eupatoria* example (population B). Point estimates are compared with sampling-distribution summaries to show how pooling/averaging changes central tendency and uncertainty relative to the single-MPM case.

Parameter	Median	Lower 95%	Upper 95%	Point estimate
Life expectancy (l_0)	1.920	1.69	2.16	1.930
Pop. growth rate (λ)	0.929	0.82	1.03	0.958
Damping ratio (ρ)	1.430	1.25	1.68	1.370

939 Table S3. Analysis 1 posterior summary for the slope parameter (β) in the life expectancy-shape
940 model. The uncertainty-aware model shows greater posterior support for $\beta > 0$ than the point-
941 estimate model.

Model	Median beta	Lower 95%	Upper 95%	P(beta > 0)
Model using point estimates	-0.017	-0.053	0.017	0.146
Model with sampling uncertainty	0.011	-0.017	0.038	0.770

942

Table S4. Analysis 2 Gaussian-process regression coefficients (monthly lags) for recruitment responses to temperature anomalies. Lag-specific posterior summaries are similar between point-estimate and uncertainty-aware model formulations.

Lag	Model	Median beta	Lower 95%	Upper 95%	lag_err
1	Point estimates	-0.251	-0.659	0.154	0.82
2	Point estimates	-0.135	-0.472	0.223	1.82
3	Point estimates	-0.030	-0.358	0.282	2.82
4	Point estimates	0.078	-0.261	0.396	3.82
5	Point estimates	0.155	-0.196	0.474	4.82
6	Point estimates	0.207	-0.156	0.507	5.82
7	Point estimates	0.272	-0.040	0.563	6.82
8	Point estimates	0.331	0.055	0.608	7.82
9	Point estimates	0.320	0.054	0.538	8.82
10	Point estimates	0.245	-0.068	0.482	9.82
11	Point estimates	0.200	-0.154	0.460	10.80
12	Point estimates	0.145	-0.151	0.416	11.80
13	Point estimates	0.111	-0.154	0.407	12.80
14	Point estimates	0.049	-0.195	0.411	13.80
15	Point estimates	-0.003	-0.251	0.421	14.80
16	Point estimates	-0.091	-0.333	0.197	15.80
17	Point estimates	-0.182	-0.464	0.084	16.80
18	Point estimates	-0.203	-0.543	0.046	17.80
19	Point estimates	-0.203	-0.494	0.044	18.80
20	Point estimates	-0.159	-0.393	0.062	19.80
21	Point estimates	-0.082	-0.306	0.181	20.80
22	Point estimates	-0.009	-0.278	0.291	21.80
23	Point estimates	0.018	-0.317	0.361	22.80
24	Point estimates	-0.002	-0.451	0.414	23.80
1	Sampling uncertainty	-0.274	-0.735	0.189	1.18

Lag	Model	Median beta	Lower 95%	Upper 95%	lag_err
2	Sampling uncertainty	-0.163	-0.551	0.236	2.18
3	Sampling uncertainty	-0.035	-0.402	0.329	3.18
4	Sampling uncertainty	0.079	-0.265	0.464	4.18
5	Sampling uncertainty	0.162	-0.197	0.517	5.18
6	Sampling uncertainty	0.225	-0.136	0.554	6.18
7	Sampling uncertainty	0.295	-0.038	0.615	7.18
8	Sampling uncertainty	0.348	0.061	0.631	8.18
9	Sampling uncertainty	0.342	0.078	0.571	9.18
10	Sampling uncertainty	0.277	-0.068	0.543	10.20
11	Sampling uncertainty	0.216	-0.161	0.497	11.20
12	Sampling uncertainty	0.155	-0.204	0.456	12.20
13	Sampling uncertainty	0.117	-0.168	0.401	13.20
14	Sampling uncertainty	0.053	-0.215	0.448	14.20
15	Sampling uncertainty	-0.004	-0.270	0.406	15.20
16	Sampling uncertainty	-0.100	-0.338	0.207	16.20
17	Sampling uncertainty	-0.182	-0.473	0.068	17.20
18	Sampling uncertainty	-0.226	-0.568	0.069	18.20
19	Sampling uncertainty	-0.226	-0.548	0.043	19.20
20	Sampling uncertainty	-0.193	-0.413	0.054	20.20
21	Sampling uncertainty	-0.112	-0.356	0.183	21.20
22	Sampling uncertainty	-0.043	-0.333	0.335	22.20
23	Sampling uncertainty	-0.020	-0.376	0.362	23.20
24	Sampling uncertainty	-0.013	-0.456	0.416	24.20

946

947 Table S5. Analysis 2 posterior summary for the spring-temperature coefficient. Point-estimate
948 and uncertainty-aware models yield similar medians and interval widths, indicating limited effect
949 of uncertainty propagation on this coefficient.

Model	Median	Lower 95%	Upper 95%
Point estimates	1.12	0.135	2.10
Sampling uncertainty	1.21	0.151	2.33

950

951 Table S6. Primary studies represented in the analysis subset, as identified in COMPADRE. For
952 matrix-level metadata and source-link details beyond this summary, refer to the COMPADRE
953 database record for each study.

Authors	Year	Journal	DOI	Species (COMPADRE label)
Andrello	2010			Dracocephalum_austriacum
Dangremond; Knight	2010	Ecology	10.1890/09-0418.1	Lupinus_tidestromii
Davison; Jacquemyn; Adriaens; Honnay; de Kroon; Tuljapurkar	2010	J Ecol	10.1111/j.1365-2745.2009.01611.x	Anthyllis_vulneraria
Fortini; Zarin	2010	Forest Ecol Manag	10.1016/j.foreco.2010.11.007	Callycophyllum_spruceanum; Carapa_guianensis; Licania_heteromorpha; Licaria_mahuba; Mora_paraensis; Platymiscium_filipes; Virola_surinamensis
Gaoue; Ticktin	2010	Conserv Biol	10.1111/j.1523-1739.2009.01345.x	Khaya_senegalensis
Jacquemyns; Brys; Jongejans	2010	Ecology	10.1890/08-2321.1	Orchis_purpurea
Picard; Mortier; Chagneau	2010	Ecol Model	10.1016/j.ecolmodel.2010.06.010	Dicorynia_guianensis
Sampaio; Scariot	2010	J Trop Ecol	10.1017/S0266467409990599	Geonoma_schottiana
Sletvold; Øien; Moen	2010	Biol Conserv	10.1016/j.biocon.2009.12.017	Dactylorhiza_lapponica
Bullock; White; Prudhomme; Tansey; Perea; Hooftman	2011	J Ecol	10.1111/j.1365-2745.2011.01910.x	Cirsium_acaule_2
Chen; Visser; Jongejans; van Breugel; Zuidema; Kassim; de Kroon	2011	J Ecol	10.1111/j.1365-2745.2011.01825.x	Shorea_leprosula
Csergő; Molnár; García	2011	Popul Ecol	10.1007/s10144-010-0249-y	Saponaria_bellidifolia
Dominguez Lozano; Moreno Saiz; Schwartz	2011	J Nat Conserv	10.1016/j.jnc.2011.05.005	Vella_pseudocytisus_subsp._paui_2

Authors	Year	Journal	DOI	Species (COMPADRE label)
Navarro; Galeano; Bernal	2011	Trop Conserv Sci	10.1177/194008291100400104	Lepidocaryum_tenue
Norghauer; Newbery	2011	Ecol Monogr	10.1890/10-2268.1	Microberlinia_bisulcata; Tetraberlinia_bifoliolata
Thorpe; Stanley; Kayne; Latham	2011			Cypripedium_fasciculatum
Andrello; Bizoux; Barbet-Massin; Gaudeul; Nicolè; Till-Bottraud	2012	Biol Conserv	10.1016/j.biocon.2011.12.012	Eryngium_alpinum
Ellis	2012	Ecology	10.1890/11-1052.1	Liatris_scariosa
Ellis; Williams; Lesica; Bell; Bierzychudek; Bowles; Crone; Doak; Ehrlén; Ellis-Adam; McEachern; Ganesan; Latham; Luijten; Kaye; Knight; Menges; Morris; den Nijs; Oostermeijer; Quintana-Ascencio; Shelly; Stanley; Thorpe; Ticktin; Valverde; Weekley	2012	Ecology	10.1890/11-1052.1	Cirsium_pitcheri_4; Phyllanthus_emblica_3
Scanga; Leopold	2012	Biol Conserv	10.1016/j.biocon.2012.01.061	Trollius_laxus
Ticktin; Ganesan; Paramesha; Setty	2012	J Appl Ecol	10.1111/j.1365-2664.2012.02156.x	Phyllanthus_emblica_2; Phyllanthus_indofischeri
Gornish	2013			Pityopsis_aspera
Matlaga; Davis	2013	J Appl Ecol	10.1111/1365-2664.12057	Miscanthus_giganteus
Osunkoya; Perrett; Fernando; Clark; Raghu	2013	Popul Ecol	10.1007/s10144-013-0364-7	Lantana_camara

Authors	Year	Journal	DOI	Species (COMPADRE label)
Villellas; Ehrlén; Olesen; Braza; García	2013	Ecography	10.1111/j.1600-0587.2012.07425.x	Plantago_coronopus_2
Scanga	2014	Plant Ecol	10.1007/s11258-014-0344-9	Trollius_laxus_2
Baldauf; Correa; Ferreira; Santos	2015	Forest Ecol Manag	10.1016/j.foreco.2015.06.022	Himatanthus_drasticus
Gibert; Magda; Hazard	2015	PLOS ONE	10.1371/journal.pone.0139919	Festuca_eskia
Berry; Natalie L Cleavitt	2021	Popul Ecol	10.1002/1438-390X.12092	Platanthera_macrophylla_; Platanthera_orbiculata_

954

Table S7. Analysis 3 site coverage and spring-temperature effect summaries for *Astragalus scaphoides*. Point-estimate and sampling-uncertainty models give similar spring-temperature coefficients within each site, showing that between-site heterogeneity is larger than within-site method differences.

Site	Years (total)	Years (modelled)	Years excluded	Spring beta (point)	Spring beta (sampling)
Haynes Creek	11	8	3	-0.441	-0.424
Sheep Corral Gulch	11	10	1	0.244	0.258
McDevitt Creek	9	9	0	-0.238	-0.212

960 Table S8. Analysis 3 posterior summary for the spring-temperature coefficient by site and model
961 formulation. Across all sites, 95% intervals overlap zero under both formulations, showing
962 similar uncertainty conclusions with and without explicit sampling-uncertainty propagation.

Site	Model	Median	Lower 95%	Upper 95%
Haynes Creek	Point-estimate model	-0.441	-1.76	0.899
Haynes Creek	Sampling-uncertainty model	-0.424	-1.74	0.872
McDevitt Creek	Point-estimate model	-0.238	-1.45	1.110
McDevitt Creek	Sampling-uncertainty model	-0.212	-1.52	1.160
Sheep Corral Gulch	Point-estimate model	0.244	-1.69	2.100
Sheep Corral Gulch	Sampling-uncertainty model	0.258	-1.51	2.080

963

964 Table S9. Analysis 2 stage-specific survival-temperature coefficients under two point-estimate
965 weighting scenarios. "No weights" treats annual stage-specific survival proportions equally,
966 whereas "SSD weights" applies stable-stage-distribution weights from the annual U matrix.

Stage	Weighting	Years used	Median	Lower 95%	Upper 95%
Stage 1	No weights	4			
Stage 1	SSD weights	4			
Stage 2	No weights	12	0.235	-0.221	0.691
Stage 2	SSD weights	12	0.093	-0.670	0.856
Stage 3	No weights	12	0.238	-0.315	0.791
Stage 3	SSD weights	12	0.178	-0.353	0.708
Stage 4	No weights	12			
Stage 4	SSD weights	12			

967

Table S10. Analysis 3 stage-specific survival-temperature coefficients under two point-estimate weighting scenarios across sites. The comparison shows how coefficient estimates and interval widths change when no stage sample-size information is used and SSD weights are substituted.

Site	Stage	Weighting	Years used	Median	Lower 95%	Upper 95%
Haynes Creek	Stage 1	No weights	8			
Haynes Creek	Stage 1	SSD weights	8			
Haynes Creek	Stage 2	No weights	8	0.180	-0.401	0.761
Haynes Creek	Stage 2	SSD weights	8	-0.103	-0.748	0.542
Haynes Creek	Stage 3	No weights	8	0.232	-0.207	0.670
Haynes Creek	Stage 3	SSD weights	8	0.232	-0.369	0.833
Haynes Creek	Stage 4	No weights	7	-0.210	-0.625	0.206
Haynes Creek	Stage 4	SSD weights	7	-0.093	-0.745	0.559
Haynes Creek	Stage 5	No weights	8	0.028	-0.702	0.759
Haynes Creek	Stage 5	SSD weights	8	0.102	-0.372	0.577
McDevitt Creek	Stage 1	No weights	9	0.120	-0.485	0.725
McDevitt Creek	Stage 1	SSD weights	9	0.164	-1.030	1.350
McDevitt Creek	Stage 2	No weights	9	0.020	-0.601	0.642
McDevitt Creek	Stage 2	SSD weights	9	0.104	-0.881	1.090
McDevitt Creek	Stage 3	No weights	9	0.086	-0.605	0.777
McDevitt Creek	Stage 3	SSD weights	9	-0.152	-0.982	0.678
McDevitt Creek	Stage 4	No weights	9	-0.211	-0.608	0.186
McDevitt Creek	Stage 4	SSD weights	9	-0.152	-0.953	0.648
McDevitt Creek	Stage 5	No weights	9	0.283	-0.371	0.937
McDevitt Creek	Stage 5	SSD weights	9	0.248	-0.160	0.657
Sheep Corral Gulch	Stage 1	No weights	10			
Sheep Corral Gulch	Stage 1	SSD weights	10			
Sheep Corral Gulch	Stage 2	No weights	10	-0.317	-0.889	0.255
Sheep Corral Gulch	Stage 2	SSD weights	10	-0.513	-0.938	-0.089
Sheep Corral Gulch	Stage 3	No weights	10	-0.460	-1.010	0.092

Site	Stage	Weighting	Years used	Median	Lower 95%	Upper 95%
Sheep Corral Gulch	Stage 3	SSD weights	10	-0.247	-0.892	0.398
Sheep Corral Gulch	Stage 4	No weights	10	0.329	-0.877	1.530
Sheep Corral Gulch	Stage 4	SSD weights	10	0.520	-1.050	2.090
Sheep Corral Gulch	Stage 5	No weights	10	-1.010	-2.220	0.204
Sheep Corral Gulch	Stage 5	SSD weights	10	-0.098	-2.070	1.880

971

Supplementary Figures

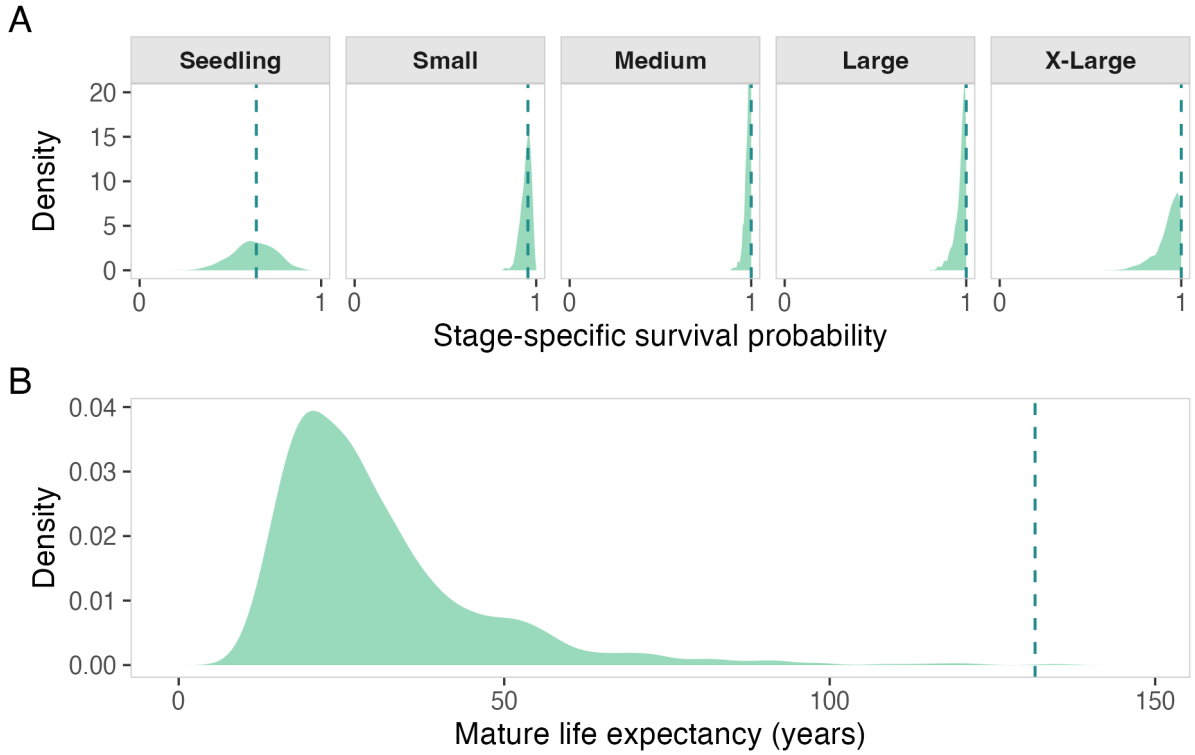

Figure 7: Boundary-estimate diagnostic. Purple lines indicate point-estimate-derived quantities and green densities indicate uncertainty-aware summaries from sampling distributions. When stage-specific survival estimates are near 0 or 1, derived-parameter sampling distributions can be displaced relative to point estimates, indicating potential inferential fragility.

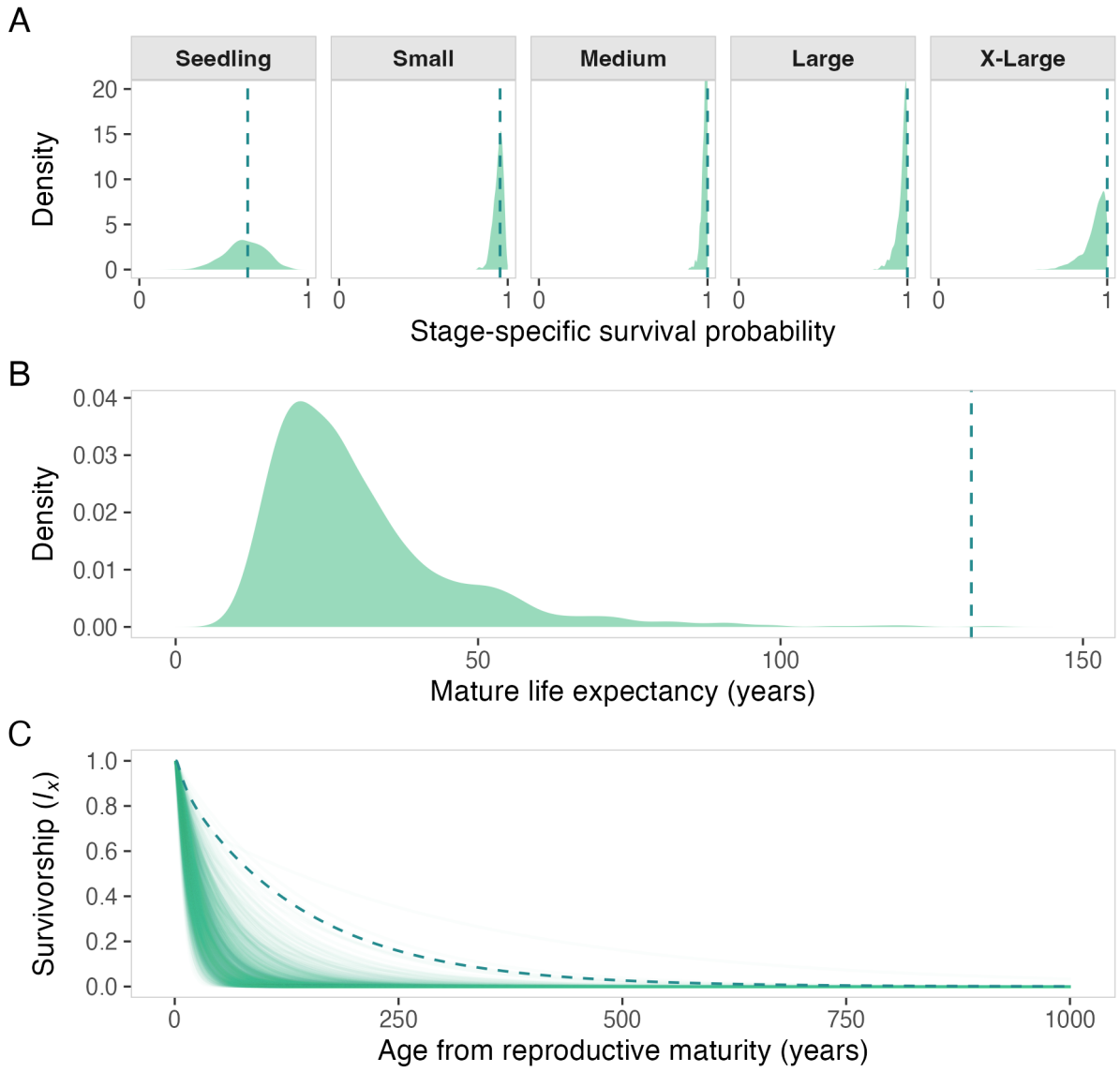

979

980 *Figure 8: Illustration of survivorship trajectories under boundary survival transitions. Age/time is shown in years.*

981 *These cases can induce artefactual trajectory shapes and help explain mismatches between point estimates and*

982 *uncertainty-aware summaries.*

983

984